EARTH SCIENCES
RESEARCH JOURNAL

Earth Sci. Res. J. Vol. 25, No. 3 (Septiembre, 2021): 309-321

UNIVERSIDAD NACIONAL DE COLOMBIA

SEISMOLOGY

The 20 July 2017 Bodrum-Kos Earthquake (Mw 6.6) in southwestern Anatolia, Turkey

Semir Över[1], Süha Özden[2], Esra Kalkan Ertan[3], Fatih Turhan[3], Zeynep Coşkun[3], Ali Pınar[3]
[1]Iskenderun Technical University, Department of Civil Engineering, 31200, Iskenderun, Turkey.
[2]Çanakkale Onsekiz Mart University, Department of Geological Engineering, 17100, Çanakkale, Turkey.
[3]Boğaziçi University, Kandilli Observatory, and Earthquake Research Institute, 36684, İstanbul, Turkey.
Corresponding Author: semir.over@iste.edu.tr

ABSTRACT

A 6.6 (Mw) earthquake struck the western part of Gökova Gulf in the eastern Aegean Sea on July 20, 2017. The fault plane solution for the mainshock shows an E-W striking normal fault with approximately N-S (N4°E) tensional axis (T-axis). Fault plane solutions for 33 aftershocks offer two groups of normal faulting with E-W and NE-SW to ENE-WSW orientations. The inversion of the focal mechanisms of the aftershocks yields two different extensional stress regimes. The stress regime obtained from 12 focal mechanisms of aftershocks and the mainshock is characterized by an approximately N-S (N5°E) σ3 axis, while the other regime calculated from 21 focal mechanisms of aftershocks exhibits σ3 axis in an NW-SE (N330°E) direction. The latter extension significantly affects the basin's growth in the area where the earthquake occurred. Twenty-four focal mechanisms of earthquakes in and around Gökova Basin before the 2017 earthquake (1933-2017) were included in the inversion to determine the stress state effective in a larger area. The inversion yielded an extensional stress regime characterized by approximately N-S (N356°E) σ3 axis. E-W trending faults inferred in the central part of Gökova Fault Zone, bordering Gökova Gulf in the north, also indicate N-S extension. The NW-SE extension obtained from NE-SW aftershocks appears to be locally effective in the northwest of Gökova Gulf. N-S extension, which appears to act on a regional scale, may be attributed to geodynamic effects related to the roll-back of the African subduction beneath the Aegean.

Keywords: Bodrum; Kos; Earthquake; Normal Fault; Inversion; Extension

Terremoto de magnitud 6.6 en Bodrum-Kos, el 20 de julio de 2017, en el suroeste de Anatolia, Turquía

RESUMEN

Un terremoto de magnitud 6.6 golpeó la parte oeste del golfo de Gökova en el este del mar Egeo el 20 de julio de 2017. El mecanismo focal del evento principal muestra un movimiento E-O en la falla normal con un eje tensional (T-axis, en inglés) en dirección N-S (N4°E). El mecanismo focal de 33 réplicas muestra dos grupos de fallamiento normal con orientaciones E-O y NE-SO hacia ENE-OSO. La inversión del mecanismo focal de las réplicas produjo dos regímenes de fuerza extensiva diferentes. El régimen de fuerza obtenido a través de 12 mecanismos focales de réplicas y del movimiento principal se caracteriza por un desplazamiento aproximado N-S (N5°E) σ3 del eje, mientras que el otro régimen se calculó a partir de 21 mecanismos focales en réplicas y muestra un desplazamiento del eje en dirección NO-SE (N330°E). Esta última extensión afecta significativamente el crecimiento de la cuenca en el área donde ocurrió el terremoto. Veinticuatro mecanismos focales de terremotos en la zona de la cuenca Gökova y que ocurrieron entre 1933 y 2017 fueron incuidos en la inversión para determinar el estado de la fuerza efectiva en una área mayor. La inversión dio como resultado un régimen de fuerza extensiva caracterizada por un desplazamiento del eje aproximado N-S (N356°E) σ3. De las fallas con tendencia E-O se infiere que en la parte central de la Zona de Fallas de Gökova, que limita al norte con el golfo de Gökova, también tiene una extensión N-S. La extensión NO-SE obtenida de las replicas NE-SO aparece como localmente efectiva en el noroeste del golfo de Gökova. La extensión N-S, que según los resultados actúa a escala regional, puede ser atribuido a los efectos geodinámicos relacionados con el retroceso de la subducción africana bajo el Egeo.

Palabras clave: Bodrum; Kos; Terremoto; Falla normal; Inversión; Extensión;

Record
Manuscript received: 07/05/2020
Accepted for publication: 16/07/2021

How to cite item
Over, S., Ozden, S., Kalkan, E. E., Turhan, F., Coskun, Z., & Pinar, A. The 20 July 2017 Bodrum-Kos Earthquake (Mw 6.6) in southwestern Anatolia, Turkey. *Earth Sciences Research Journal*, 25(3), 309-321. DOI: https://doi.org/10.15446/esrj.v25n3.87080

Introduction

Plate boundary forces caused by relative movements between Africa, Arabia, and Eurasia resulted in complex tectonic structures in the western Anatolia-Aegean region (Fig. 1). Plate movements involving the convergence of Arabia and Africa with Eurasia in the north; 1) give rise to the westward extrusion of Anatolia along the strike-slip North Anatolian Fault (NAF) and East Anatolian Fault (EAF), 2) cause crustal extension in western Anatolia-Aegean, and 3) are responsible for complex deformation in the Eastern Mediterranean region (McKenzie, 1972; Dewey and Şengör, 1979; Le Pichon and Angelier, 1979; Angelier et al., 1981; Jackson and McKenzie, 1984, 1988; Taymaz et al., 1990; 1991; Över et al., 2010; Özden et al., 2018). The complex tectonics of western Anatolia-Aegean involve different extensional regimes: N-S, NE-SW, and NW-SE (McKenzie, 1972; Jolivet and Brun, 2010; Alçiçek et al., 2006; Shah, 2015; Över et al., 2016; Ocakoğlu et al., 2018).

Gökova Gulf, which runs east-west, is an asymmetrical basin that is growing towards the sea. The Gökova Graben formed on the Lycian Nappes and filled with Plio-Quaternary units known as the Gökova Formation (Görür et al., 1995; Gürer and Yılmaz, 2002; Gürer et al., 2013; Tur et al., 2015). Gürer et al. (2013) suggested that the northern edge of the gulf is bounded by the south-dipping E-W Gökova Fault, one of the most active structures in the southern part of west Anatolia-Aegean, based on geomorphological and geological features. The southern border of the basin is not as clear and uninterrupted as the northern border. The active fault map also shows that the Datça Fault Zone, which represents the western part of the southern boundary of the basin, is more active (Fig. 2). The Datça Fault Zone is divided into two parts: north and south. The northern segment extends to the east of Kos (Karasözen et al., 2018), while the southern segment is listric (Kurt et al., 1999). Analyzing both bathymetric and seismic reflection data, İşcan et al. (2013) revealed the existence of active strike-slip faults with various directions in the Gulf of Gökova. From analysis of the focal mechanisms, Shah (2015) asserted that the area is dominated by normal events with few strike-slip events at the western margin of Gökova Gulf. The interpretation of new multichannel seismic profiles by Ocakoğlu et al. (2018) also shows the existence of active strike-slip and normal faults in different directions in the Gulf of Gökova. They pointed out southern-dipping

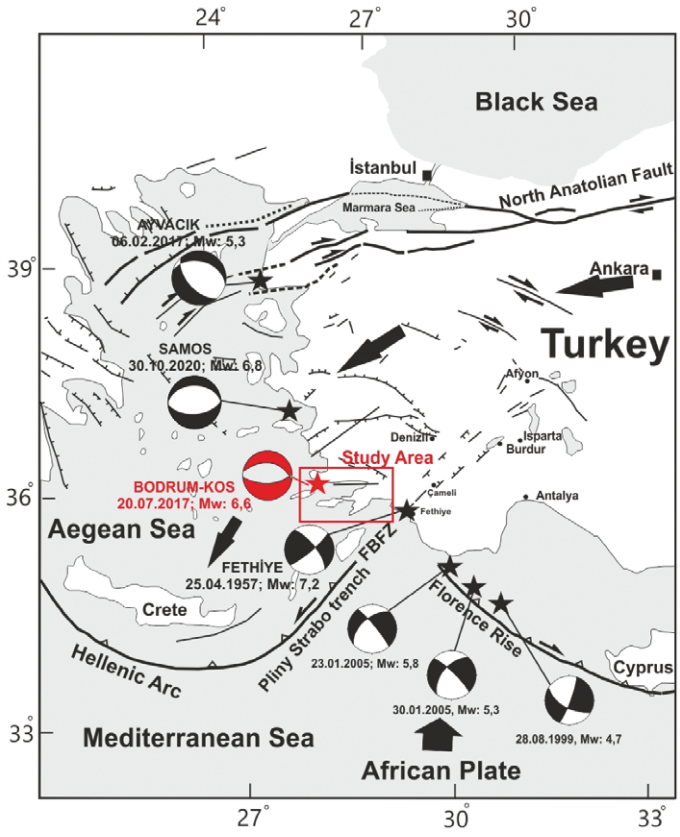

Figure 1. Map of simplified tectonic framework of the Aegean-Mediterranean Sea region (modified from Barka, 1992; Över et al., 2010).

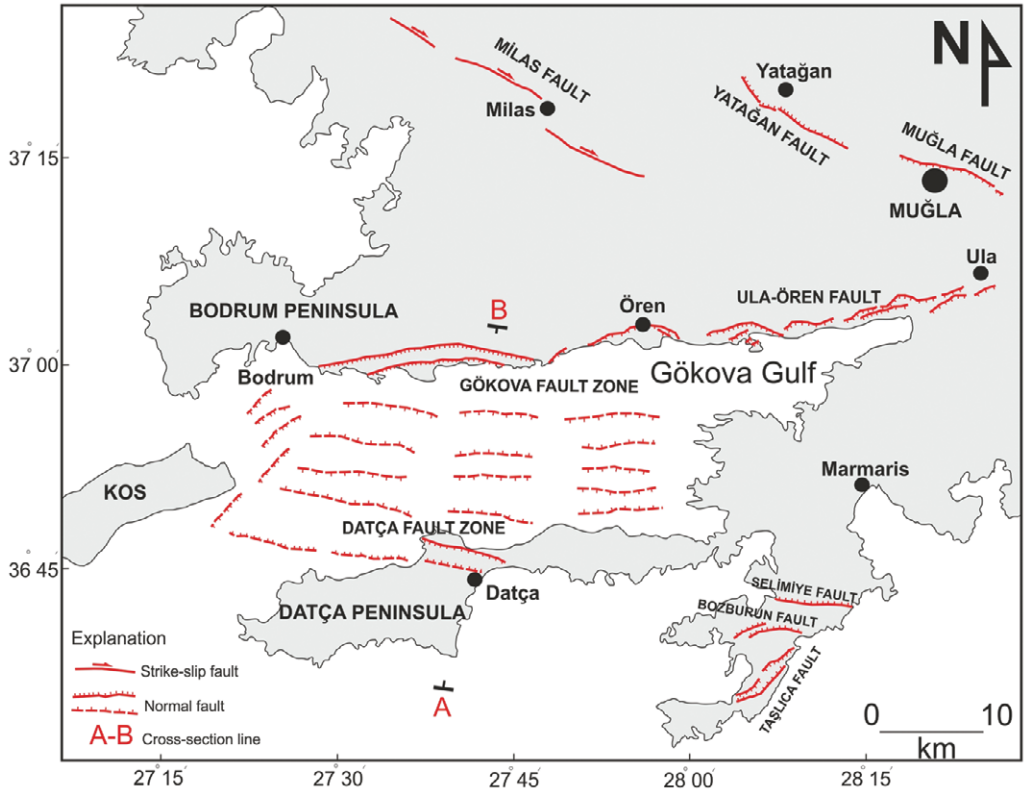

Figure 2. Location map and active faults in Gökova Gulf and surroundings (Fault data are taken from Duman, et al., 2011; Emre, et al., 2013; İşcan et al., 2013; Karasözen

et al., 2018).

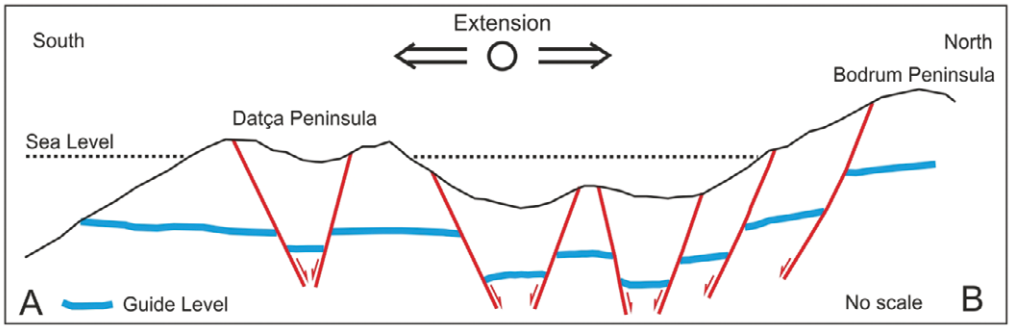

Figure 3. A cross-section of Gökova Gulf from Bodrum Peninsula to Datça (A-B section line shown in Fig 2).

normal faults on the north border (i.e. Gökova Fault Zone) and northern-dipping normal faults on the southern border of the basin (i.e. Datça Fault Zone). Normal faults were also implied in the Gökova Basin by several studies (e.g., Kurt et al., 1999; Uluğ et al., 2005; İşcan et al., 2013; Tur et al., 2015; Ocakoğlu et al., 2018).

Following the earthquake on July 20, 2017, researchers obtained contrary findings about the source fault and the fault's dip direction: (1) from geophysical and geodetic data the Bodrum-Kos earthquake ruptured a south-dipping E-W normal fault (Saltogianni et al., 2017; Tiryakioğlu et al., 2018; Ocakoğlu et al., 2018) or (2) a north-dipping E-W normal fault (Karasözen et al., 2018; Ganas et al., 2019; Konca et al., 2019). Karasözen et al. (2018) asserted that the source fault was the northern Datça Fault. A section of Gökova Bay extending from the Bodrum Peninsula to the Datça Peninsula shows the presence of E-W striking faults dipping both south and north (Fig. 3).

In the last 30 years, GPS studies about the tectonics of the Eastern Mediterranean have yielded important results, including: 1) the velocity and direction of movement of Africa and Arabia relative to Eurasia (McClusky et al., 2000; Reilinger et al., 2006), 2) the rate and direction of movement of Anatolia towards the west relative to Eurasia along the dextral NAF (North Anatolian Fault) and sinistral EAF (East Anatolian Fault) (McClusky et al., 2000; Reilinger et al., 2006), 3) rate and direction of motion in west Anatolia-Aegean toward the Hellenic Trench (McClusky et al., 2000; Aktuğ et al., 2009; Howell et al., 2017), and 4) the crustal extension in the west Anatolia-Aegean (LePichon et al., 1995; McClusky et al., 2000; Reilinger et al., 2010). This area is currently undergoing a N-S extensional process at a rate of 30-40 mm/yr, which is well documented (Oral et al., 1995; LePichon et al., 1995), 6) the determination of both earthquake parameters and the source fault geometry (Saltogianni et al., 2017; Tiryakioğlu et al., 2018; Karasözen et al., 2018), and finally 7) revealed the coseismic deformation of the 20th July Bodrum-Kos earthquake (Tiryakioğlu et al., 2018). The GPS velocity vectors calculated relative to Anatolia (fixed) indicate an increase in the velocity of the southwestward extrusion of Anatolia in western Turkey and the Aegean region compared to other areas of Turkey accompanied by anticlockwise rotation (McClusky et al., 2000; Howell et al., 2017).

To define the stress regimes and their tectonic implications, we used a method proposed by Carey-Gahillardis and Mercier (1987). We introduced the focal mechanisms of both the main shock and its aftershocks into the inversion algorithm. We also compiled the published focal mechanisms of earthquakes that occurred in Gökova and its environs between 1933 and 2017 in order to

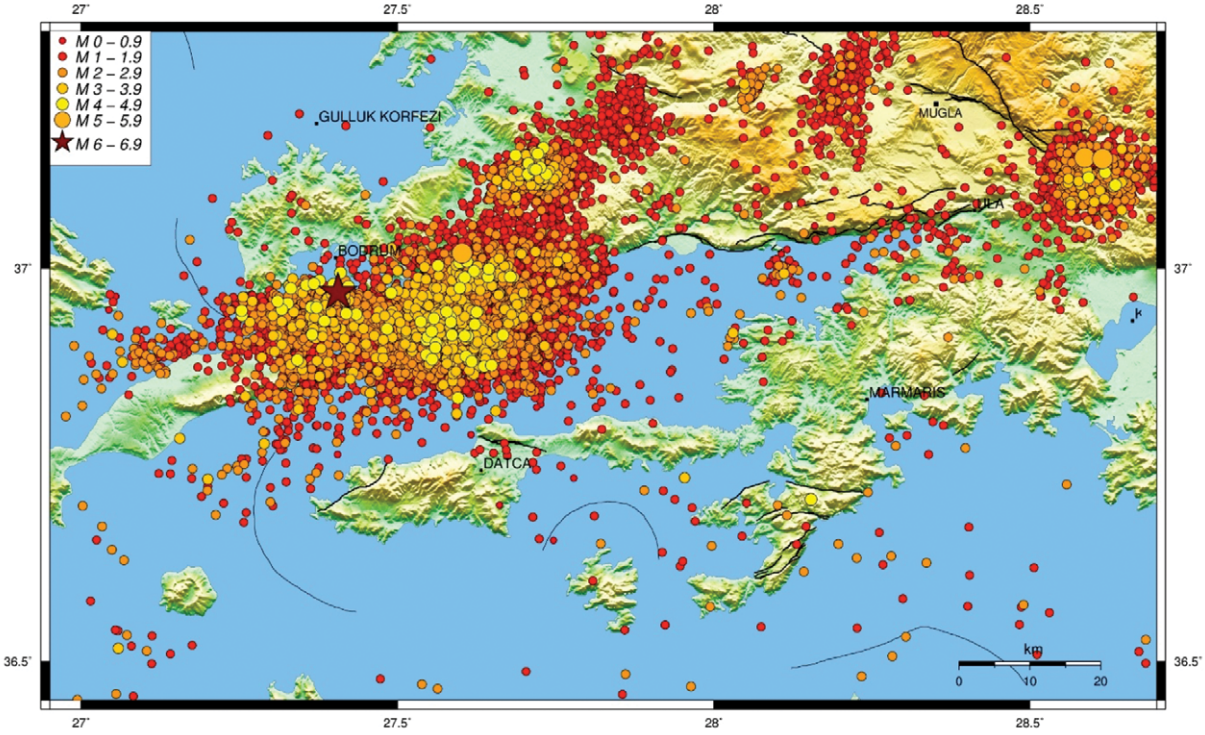

Figure 4. Map of the distribution of earthquake (20 km depth) epicenters between 20.07.2017 and 20.02.2018 in Gökova Gulf. The earthquakes are compiled from KOERI.

determine the tectonic regime responsible for the great Bodrum-Kos Earthquake in terms of regional significance.

Seismicity

The historical catalogues show that Gökova Gulf and its surrounding settlements have been hit many times by a number of moderate to major destructive earthquakes, such as in 24 BC, 412 BC (Ambraseys and White, 1997), 227 BC, 199-198 BC, AD 141, 144, 174, 344, 1493, 1851, 1863, and 1869 (Ergin et al., 1967; Guidoboni et al., 1994; Yolsal et al., 2007). Luttrell (1999) reported that the city of Bodrum was totally demolished by the 1493 earthquake. The activity in the region is also confirmed by earthquakes occurring during the instrumental period, such as 23 April 1933 (Mw: 6.2), 23 May 1941 (Mw: 5.4), 13 December 1941 (Mw: 6.3), 25 April 1959 (Mw: 6.1), 19 February 1989 (Mw: 5.6), 5 October 1999 (Mw: 5.2), 4 August 2004 (Mw: 5.4), and 10 January 2005 (Mw: 5.2) (Eyidoğan and Barka, 1996; Şaroğlu et al., 1992; Uluğ et al., 2005; Yolsal and Taymaz, 2010). Kalafat and Horasan (2012) observed swarm type activity in the western Gökova Gulf during 2004 and 2005. Historical and instrumental era earthquakes show that the basin contains significant faults that enable its development. On July 20, 2017, one of the faults triggered a 6.6 (Mw) earthquake. Following the Bodrum-Kos Earthquake, more than 3000 aftershocks ranging in magnitude from 1.0 to 4.8 were recorded across Gökova Gulf according to KOERI (Kandilli Observatory and Earthquake Research Institute) data (Fig. 4). Aftershocks were scattered across a wide region, mainly in the west of the basin, and did not follow a linear distribution (Fig. 4). This event created a tsunami with a water wave reaching almost 2 meters height, which damaged the southern coast of Bodrum and the northern coast of Kos Island (Heiderzadeh et al., 2017; Yalçıner et al., 2017). Several studies reported tsunamis in relation to historical and instrumental period events (i.e. in 365, 554, 1303, 1481, 1822 and 1948) in the Eastern Mediterranean (Altınok and Ersoy, 2000; Yolsal et al., 2007; Çevikbilen and Taymaz, 2012, Çevikbilen et al., 2014).

Methodology

Moment Tensor Inversion

In this study we used Moment Tensor (MT) inversion algorithms that model the waveforms recorded at one or more 3-component broadband seismic stations (e.g., Kuge, 2003; Sokos and Zahradnik, 2008). These techniques perform waveform inversions to find source parameters of small to moderate sized earthquakes. One of the most user-friendly MT inversion routines recently adopted by Seiscmop3 is ISOLA, which is based on FORTRAN codes and offers a MATLAB graphic interface. ISOLA allows for both single and multiple point source iterative deconvolution (Kikuchi and Kanamori, 1991) and inversion of complete regional and local waveforms. In addition, we also used the technique developed by Kuge (2003). In this method, waveform fitting between the observed and synthetic displacement seismograms from one or more stations at local distances is achieved by searching for a MT point on a grid scheme for the best fit between the observed and the synthetic displacement seismograms. During the inversion process uniform weight is given to all seismograms. The broadband seismic station networks operated by KOERI, Disaster and Emergency Management Presidency (AFAD) and National Observatory of Athens (NOA) were utilized. For data selection to be used for the inversion process, firstly the signal quality check was completed for three-component broadband stations. Seismograms with gaps and signals with signal-to-noise ratio lower than 4.0 were not considered. Good azimuthal distribution of stations plays significant role in constraining the MT inversion results. The Green's function (GF) calculation is performed using the frequency-wavenumber method (Bouchon, 1981). GFs were computed using the crustal structure from Akyol et al. (2006). When GFs are calculated, the positions of epicenters are fixed, and the depth is allowed to deviate from close to the surface to a depth of up to 30 km in steps of 2 km. The quality of fit between the observed and predicted seismograms is measured by variance reduction (VR); the larger the value of VR, the better the fit. The variance reduction is calculated for various depths for each time shift, and the faulting mechanism was selected with maximum VR for the analyzed event (Fig. 5).

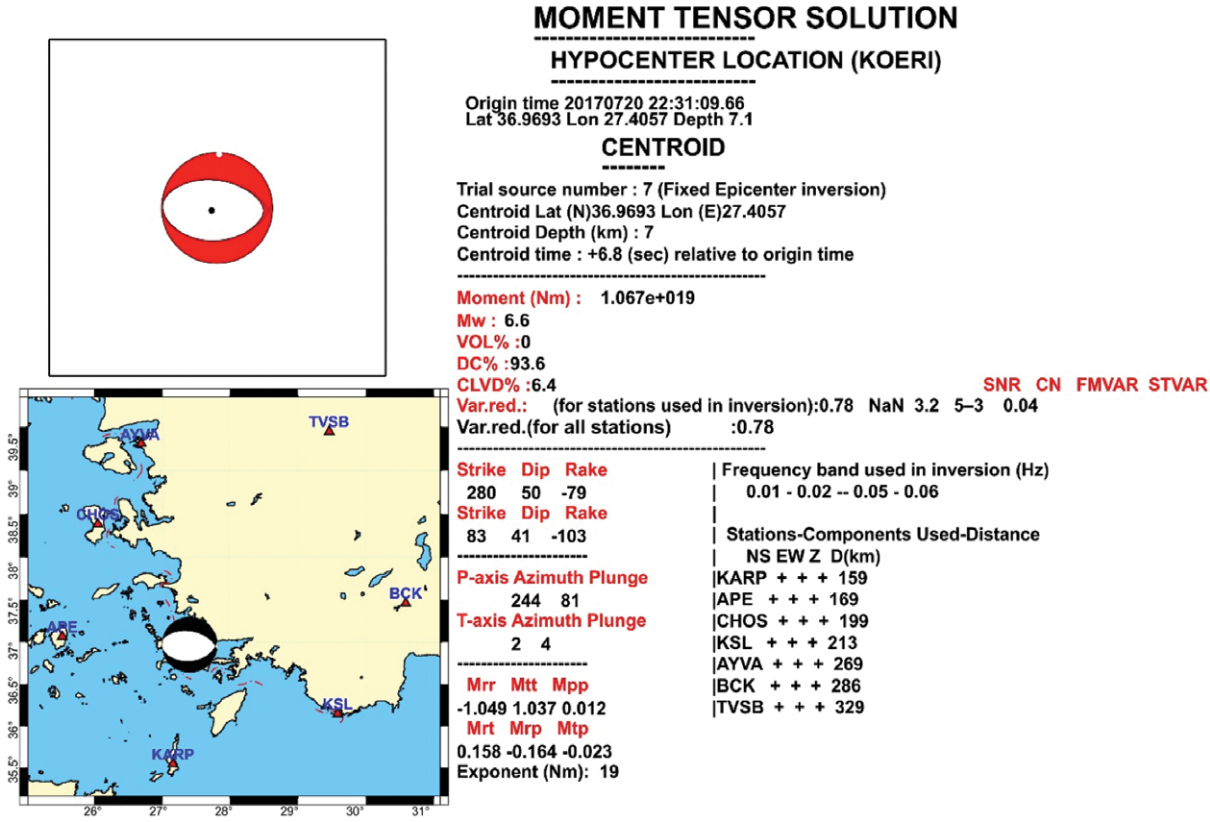

Figure 5. CMT solution result for the Mw 6.6 Bodrum-Kos earthquake (20 July 2017).

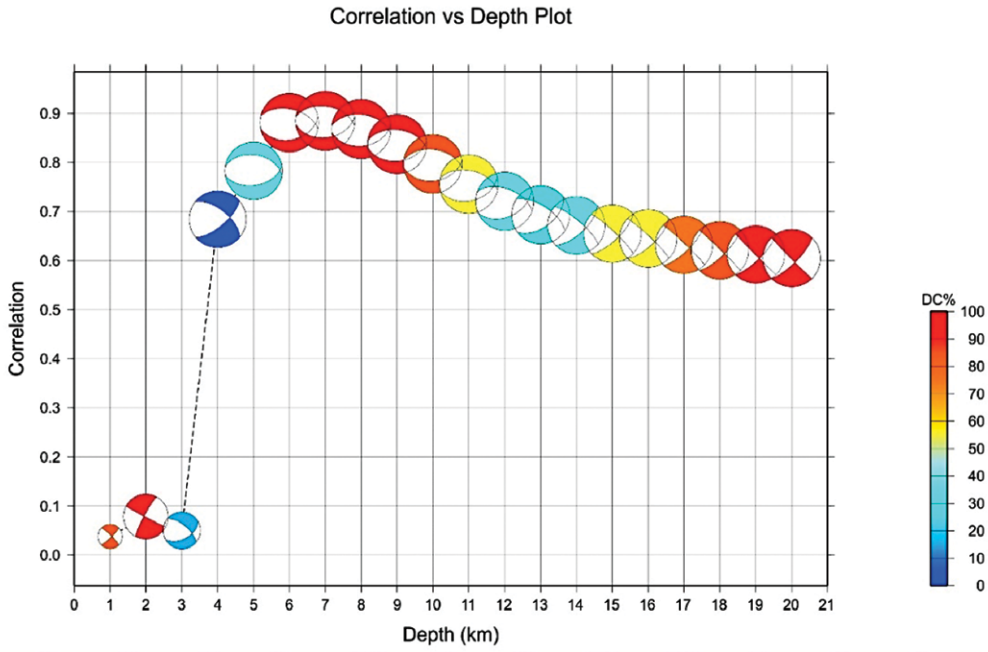

Figure 6. The correlation vs source number plot

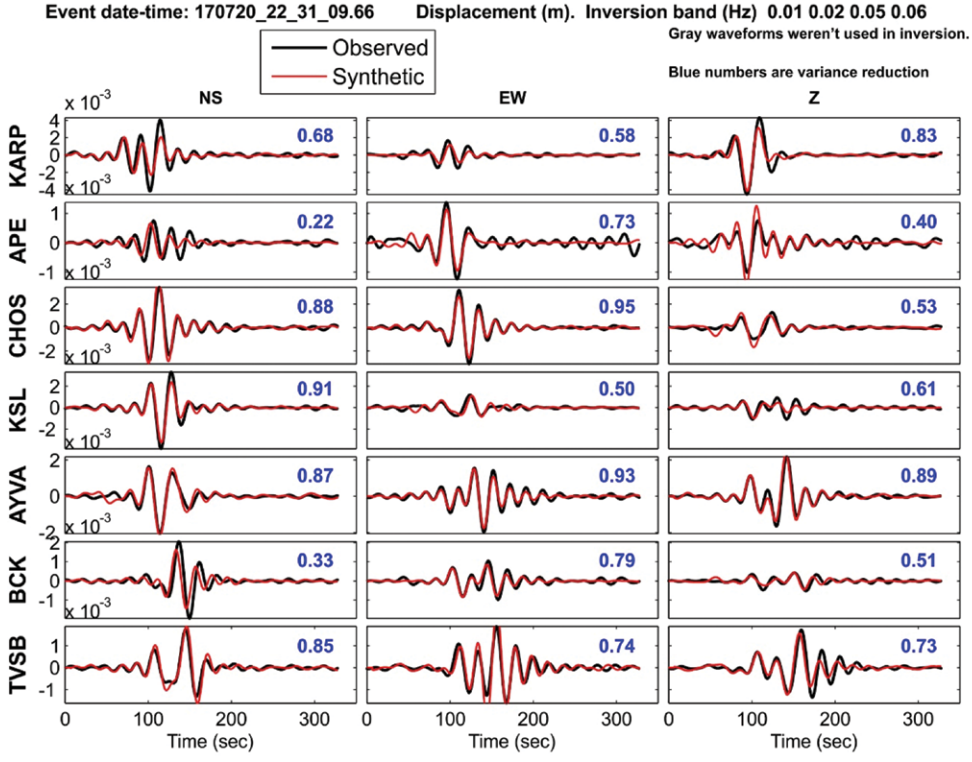

Figure 7. Observed versus synthetic waveform fits.

Inversion of seismic slip-vector data sets to determine the present-day stress state

To compute the state of stress responsible for present-day faulting from the population of focal mechanisms of earthquakes that occurred in the Gökova Gulf, we used an inversion method proposed by Carey-Gailhardis and Mercier (1987); this is one of several existing algorithms (Vasseur et al., 1983; Gephart and Forsyth, 1984). The inversion is a statistical method which allows calculation of the best mean fitting stress state from a population of focal mechanisms by selecting one of two nodal planes as the fault plane.

According to this inversion process, the slip (s, defined by a slip vector corresponding to a striation for geological data or a rake for seismological focal mechanisms) on each fault plane occurs in the direction of the resolved shear stress (t), the fault plane being a pre-existing fracture. In the case of a seismic event, the inversion computes a mean best-fitting deviatoric stress tensor by minimizing the angular deviation between an expected slip vector (maximum shear, t) and the observed slip vector (s) deduced from the focal mechanism (Carey and Brunier 1974; Carey 1979). All inversion results include the orientation (azimuth and plunge) of the principal stress axes of a mean deviatoric

stress tensor, as well as a 'stress ratio' [$R = (\sigma_2 - \sigma 1)/(\sigma_3 - \sigma_1)$], a linear quantity describing relative stress magnitudes, where the principal stress axes, $\sigma 1$, σ_2, and σ_3 correspond to compressional, intermediate, and extensional deviatoric stress axes, respectively. It is necessary to know the seismic slip vector, and consequently to select the preferred seismic fault plane for each pair of nodal planes to compute the stress state from earthquake focal mechanisms. For major earthquakes, the selection can be made if there is a co-seismic rupture, or from the spatial epicenter distribution of the aftershock sequence. There is another option for earthquake populations with low magnitude and no surface rupture-computation. It is possible to calculate the fault slip vector using Bott's (1959) model since only one of the two slip vectors of a focal mechanism solution is in accordance with the principal stress axes. For this slip vector, the R ratio, defined [$R = (\sigma_2 - \sigma_1)/(\sigma_3 - \sigma_1)$], is such that $0<R<1$ (Carey-Gailhardis and Mercier, 1987). Furthermore, unless both nodal planes of a focal mechanism converge along a principal stress axis, if one of the nodal planes meets this condition, the other does not (Carey-Gailhardis and Mercier, 1987). We used the calculation method described above to select the nodal plane of each focal mechanism in this analysis. In general, a collection of seismic event focal mechanisms leads to a well-defined assessment of the regional or local stress state that is consistent with the geologically determined stress state: that is, the stress state resulting from inversions of striae measured on fault planes (e.g., Sebrier et al., 1988; Mercier et al., 1991, 1992; Bellier and Zoback, 1995; Bellier et al., 1997; Över et al., 2010). As mentioned above, fault slip inversion schemes assume that the slip vector on each plane corresponds to the direction of the maximum resolved shear stress on that plane. The inversion involves at least four different fault

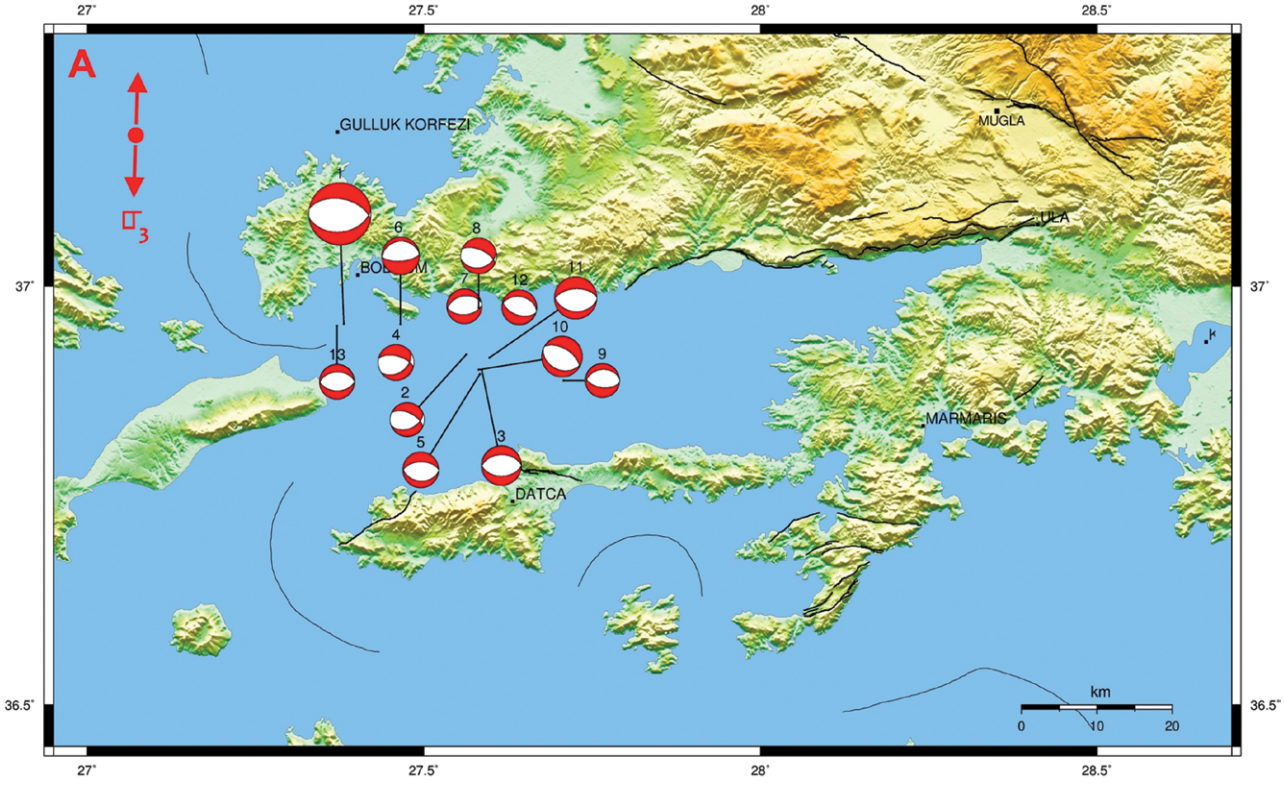

Figure 8. The moment tensor solution of the mainshock and 12 aftershocks between 20.07.2017 and 16.10.2017 in Gökova Gulf (numerical data are given for each earthquake in Table 1). Plots show nodal planes. Numbers outside the stereoplot refer to the focal mechanism labels given in Table 1.

Table 1. The parameters of the main shock (No 1) and 12 aftershocks with approximately E-W direction ($M \geq 3.6$) occurring between 20.07.2017 and 16.10.2017 in Gökova Gulf shown in Figure 8 and 11.

No	Date Day.Month. Year	Time (UTC)	Lat. N (°)	Long. E (°)	Plane 1 Strike°/Dip°/ Plunge°	Plane 2 Strike°/Dip°/ Plunge°	Mag. (Moment)	Seismic Moment (Nm)	H (km)	Variance Reduction (%)	Station Num.	References
1	20.07.2017	22:31:09	36.969	27.406	**280⁰/50⁰/-79⁰**	83⁰/41⁰/-103⁰	6.6	1.06e+19	7	78	7	This study
2	20.07.2017	22:54:35	36.933	27.588	**68⁰/44⁰/-127⁰**	293⁰/56⁰/-60⁰	3.6	2.75e+14	6	65	5	This study
3	21.07.2017	05:13:58	36.914	27.611	90⁰/46⁰/-89⁰	**269⁰/44⁰/-91⁰**	4.2	2.65e+15	6	69	6	This study
4	21.07.2017	07:05:23	36.923	27.483	284⁰/60⁰/-61⁰	**56⁰/41⁰/-130⁰**	3.8	7.03e+14	9	64	6	This study
5	21.07.2017	21:51:01	36.909	27.608	**95⁰/37⁰/-85⁰**	268⁰/53⁰/-94⁰	3.8	5.46e+14	4	80	7	This study
6	24.07.2017	21:48:48	36.969	27.490	86⁰/67⁰/-89⁰	**264⁰/23⁰/-92⁰**	4.0	1.48e+15	7	73	8	This study
7	30.07.2017	07:06:17	36.971	27.585	87⁰/50⁰/-84⁰	**258⁰/41⁰/-97⁰**	3.7	3.76e+14	7	70	6	This study
8	09.08.2017	09:25:29	36.988	27.606	**293⁰/61⁰/-72⁰**	80⁰/34⁰/-119⁰	3.8	5.58e+14	6	70	7	This study
9	12.08.2017	02:02:02	36.902	27.732	263⁰/35⁰/-102⁰	**98⁰/55⁰/-81⁰**	3.6	2.99e+14	4	63	5	This study
10	18.08.2017	12:47:31	36.914	27.606	**111⁰/34⁰/-89⁰**	289⁰/56⁰/-91⁰	4.3	4.13e+15	6	77	6	This study
11	18.08.2017	14:10:47	36.929	27.622	**267⁰/55⁰/-95⁰**	96⁰/35⁰/-83⁰	4.5	6.15e+15	10	78	6	This study
12	21.08.2017	10:43:24	36.989	27.666	279⁰/38⁰/-98⁰	**110⁰/52⁰/-83⁰**	3.7	1.40e+01	4	57	6	This study
13	16.10.2017	07:23:48	36.967	27.396	**91⁰/47⁰/-87⁰**	266⁰/43⁰/-94⁰	3.7	4.96e+14	9	79	5	This study

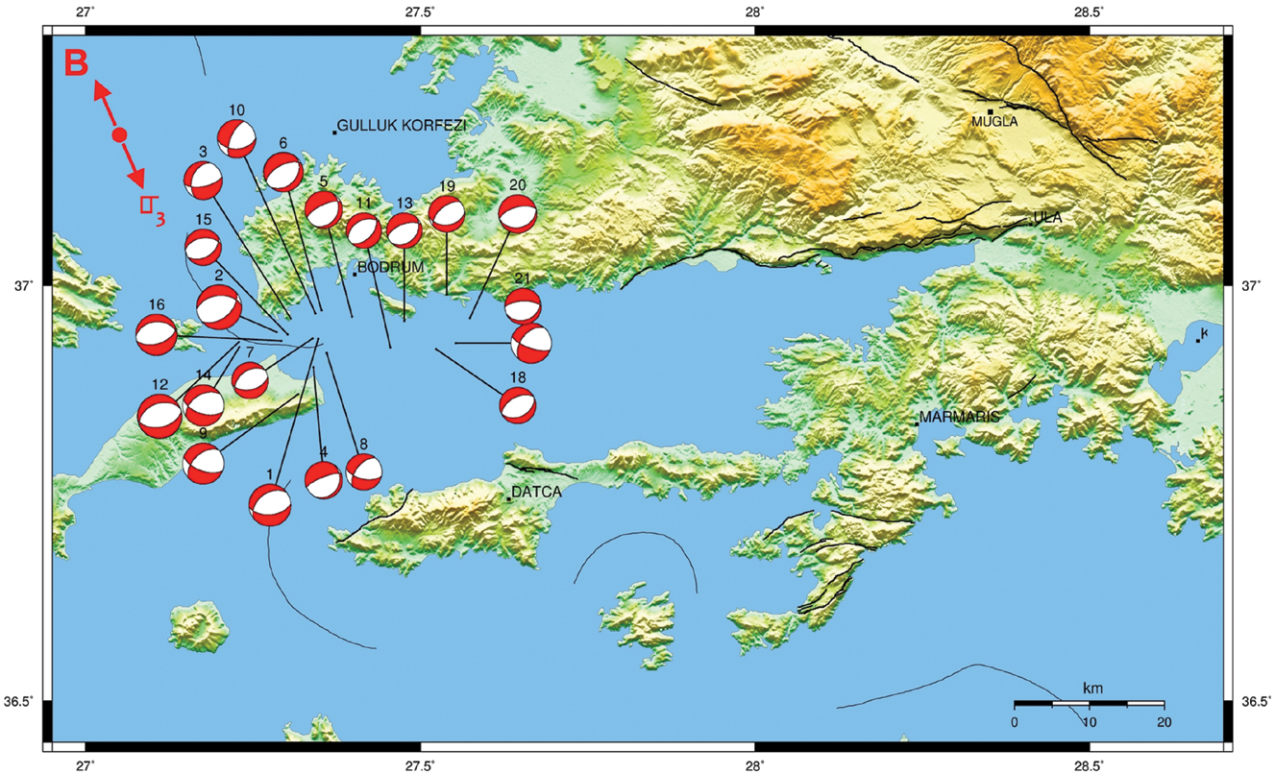

Figure 9. The moment tensor solutions of 21 aftershocks between 20.07.2017 and 09.08.2017 in Gökova Gulf (numerical data are given for each earthquake in Table 2). Plots show nodal planes. Numbers outside the stereoplot refer to the focal mechanism labels given in Table 2.

Table 2. The parameters of 21 aftershocks (M ≥ 3.8) with approximately NW-SE direction occurring between 20.07.2017 and 09.08.2017 in Gökova Gulf shown in Figures 9 and 11.

No	Date Day.Month. Year	Time (UTC)	Lat. N (°)	Long. E (°)	Plane 1 Strike°/Dip°/ Plunge°	Plane 2 Strike°/Dip°/ Plunge°	Mag. (Moment)	Seismic Moment (Nm)	H (km)	Variance Reduction (%)	Kandilli Station Num.	References
1	20.07.2017	22:52:58	36.950	27.372	85⁰/53⁰/-69⁰	233⁰/42⁰/-115⁰	4.5	6.15e+15	9	71	6	This study
2	20.07.2017	23:23:51	36.958	27.310	265⁰/47⁰/-65⁰	309⁰/48⁰/-114⁰	4.8	1.17e+17	10	68	6	This study
3	21.07.2017	00:16:40	36.974	27.331	79⁰/65⁰/-56⁰	201⁰/42⁰/-140⁰	4.1	1.54e+15	12	75	5	This study
4	21.07.2017	00:53:55	36.916	27.365	248⁰/76⁰/-80⁰	31⁰/17⁰/-126⁰	4.0	1.24e+15	7	60	7	This study
5	21.07.2017	01:25:34	36.977	27.422	244⁰/69⁰/-76⁰	29⁰/25⁰/-123⁰	4.0	1.40e+01	8	83	6	This study
6	21.07.2017	01:50:29	36.984	27.377	242⁰/60⁰/-79⁰	42⁰/32⁰/-107⁰	4.2	1.50e+01	13	77	5	This study
7	21.07.2017	01:54:46	36.951	27.364	235⁰/44⁰/-106⁰	77⁰/48⁰/-75⁰	3.9	1.40e+01	6	79	6	This study
8	21.07.2017	01:56:27	36.933	27.384	103⁰/58⁰/-42⁰	219⁰/56⁰/-140⁰	3.9	1.40e+01	9	62	6	This study
9	21.07.2017	02:12:34	36.883	27.342	226⁰/51⁰/-142⁰	110⁰/61⁰/46⁰	4.4	4.35e+15	10	72	6	This study
10	21.07.2017	05:52:13	36.981	27.368	204⁰/65⁰/-130⁰	87⁰/46⁰/-36⁰	4.1	1.54e+15	11	64	6	This study
11	21.07.2017	14:21:55	36.940	27.480	241⁰/42⁰/-77⁰	44⁰/49⁰/-101⁰	3.8	6.08e+14	5	69	7	This study
12	21.07.2017	17:09:46	36.947	27.254	249⁰/41⁰/-97⁰	78⁰/49⁰/84⁰	4.7	1.12e+16	11	63	7	This study
13	21.07.2017	23:00:48	36.972	27.501	249⁰/60⁰/-78⁰	47⁰/32⁰/-109⁰	3.8	6.81e+14	6	67	7	This study
14	22.07.2017	17:09:20	36.940	27.254	237⁰/46⁰/-130⁰	107⁰/57⁰/56⁰	4.4	4.32e+15	10	70	6	This study
15	23.07.2017	18:02:33	36.955	27.326	261⁰/48⁰/-74⁰	58⁰/44⁰/-107⁰	3.9	1.06e+15	16	56	6	This study
16	24.09.2017	16:57:16	36.948	27.317	264⁰/37⁰/-81⁰	72⁰/53⁰/-97⁰	4.4	4.75e+15	8	72	8	This study
17	21.07.2017	01:35:43	36.945	27.578	218⁰/48⁰/-153⁰	110⁰/70⁰/-45⁰	4.3	1.50e+01	6	84	7	This study
18	21.07.2017	03:55:32	36.938	27.548	64⁰/38⁰/-88⁰	241⁰/52⁰/-92⁰	3.9	8.63e+14	6	72	5	This study
19	30.07.2017	10:56:32	37.003	27.564	230⁰/56⁰/-110⁰	83⁰/39⁰/-64⁰	3.9	1.40e+01	5	77	6	This study
20	07.08.2017	05:44:24	36.975	27.599	76⁰/29⁰/-89⁰	256⁰/61⁰/-90⁰	4.1	1.62e+15	4	75	7	This study
21	09.08.2017	22:56:18	36.989	27.678	268⁰/66⁰/-81⁰	68/26/-108	3.9	9.16e+14	4	77	6	This study

sets in this case since there are four unknowns (three defining the orientation of the principal axes and one defining the stress ratio R). Faults with variable dip angles and distinct strike directions, rather than a continuum of strikes around a single mean direction, are included in ideal data sets. When the deviation angle between the measured slip vector 't' and the observed slip vector 's' is less than 20˚, the slip vector determined from a focal mechanism is usually considered to be mechanically explained by the computed stress deviator. Results of stress inversions are considered reliable if 80 percent of the deviation angles between t and s are less than 20˚ and if the computed solution is stable; that is, the inversion tends towards the same solution regardless of the initial parameter values (Carey, 1979; Carey-Gailhardis and Mercier, 1987; Mercier et al., 1989, 1991; Bellier and Zoback, 1995).

Result and Discussion

Focal Mechanisms of the Main Earthquake and Aftershocks

An earthquake (M=6.6) hit Bodrum, Kos, and the surrounding area in the west of the Gulf of Gökova on July 20, 2017. The main shock and the majority of the aftershocks show predominantly normal faulting character. The focal mechanism analysis was made using Kuge (2003)'s method and ISOLA software. The main shock (Mw: 6.6) with a N-S (N4°E) T-axis must have occurred on a relatively large E-W fault (Table 1). The MT analysis yields normal faulting mechanisms for 34 of the events occurring after the Bodrum-Kos earthquake (Mw 6.6). The focal mechanisms of the aftershocks show two distinct nodal plane directions. They are approximately E-W (Fig. 8 and Table 1) and NE-SW to ENE-WSW (Fig. 9 and Table 2), respectively. The E-W directional nodal planes indicate N-S extension, while the ones with NE-SW to ENE-WSW orientation indicate approximately NW-SE extension. Several marine geophysical and geodetic studies revealed a large number of faults, mostly normal and a few strike-slip, in the basin with varying directions (Kurt et al., 1999; Uluğ et al., 2005; İşcan et al., 2013; Tur et al., 2015; Ocakoğlu et al., 2018; Tiryakioğlu et al., 2018). Ocakoğlu et al. (2018) described NE-SW normal faults at the western end of the bay off Kos Island (their profile 3 in Fig. 11).

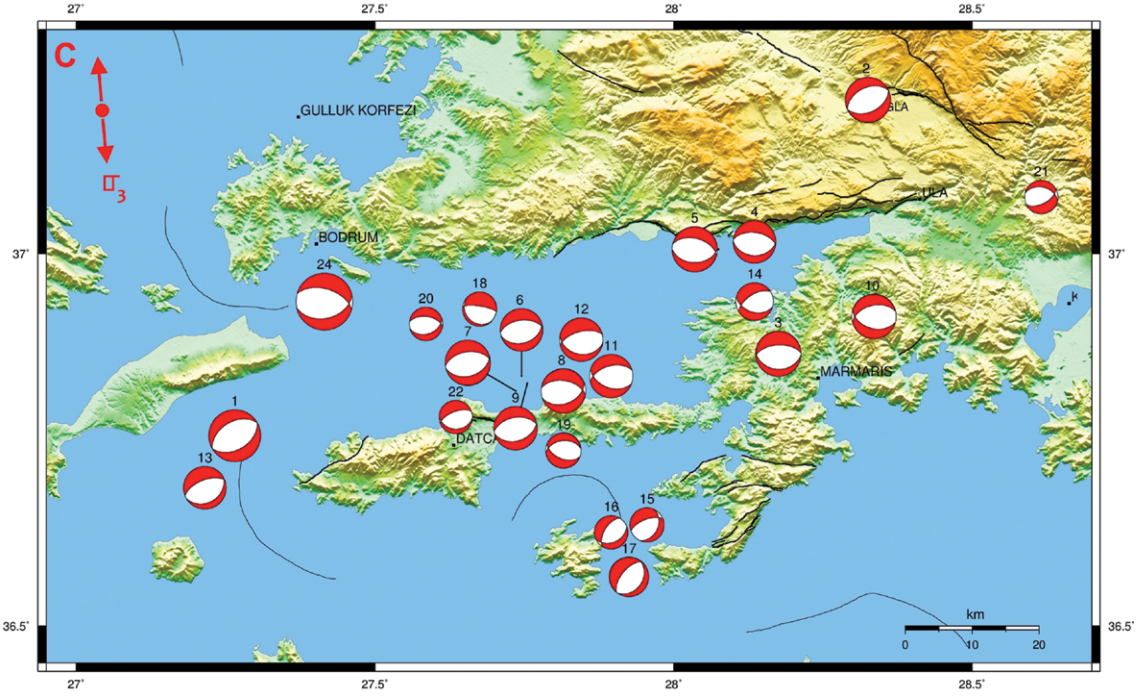

Figure 10. The moment tensor solutions of 24 historical earthquakes between 1933 and 21.07.2017 in and around Gökova Gulf (references and numerical data are given for each earthquake in Table 3). Plots show nodal planes. Numbers outside the stereoplot refer to the focal mechanism labels given in Table 3.

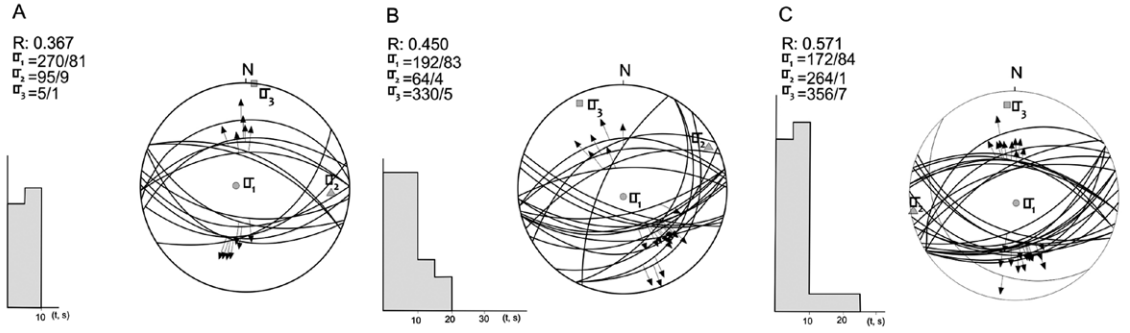

Figure 11. A. Inversion results of the earthquake slip data computed from the focal mechanisms of earthquakes shown in Figure 8 and in Table 1. (B) Inversion results of the earthquake slip data computed from the focal mechanisms of earthquakes shown in Figure 9 and in Table 2. **(C)** Inversion results of the earthquake slip data computed from the focal mechanisms of earthquakes shown in Figure 10 and in Table 3. Stress axes obtained from the inversions are shown by diamonds ($\sigma 1$), triangles ($\sigma 2$) and squares ($\sigma 3$) and stress ratio value given by the formula [$R = (\sigma 2 - \sigma 1)/(\sigma 3 - \sigma 1)$]. Thick lines on the fault traces give the deviation angle between measured (s) and predicted (τ) slip-vectors for each fault plane. Histogram shows distribution of deviation angles (angle between the observed slip, s, and the predicted slip, τ.

Table 3. The parameters of the 24 earthquakes (M ≥ 4.0) which occurred between 1933 and 2017 in and around Gökova Gulf shown in Figure 10 and 11.

No	Date Day.Month. Year	Time (UTC)	Lat. N (°)	Long. E (°)	Plane 1 Strike°/Dip°/Plunge°	Plane 2 Strike°/Dip°/Plunge°	Mag. (Moment)	H (km)	References
1	23.04.1933	05:57:37	36.77	27.29	60⁰/45⁰/-90⁰	240⁰/45⁰/-90⁰	6.2	30	Jackson, 1992
2	23.05.1941	23:00:48	37.22	28.35	65⁰/45⁰/-90⁰	245⁰/45⁰/-90⁰	5.4	48	Jackson, 1992
3	19.02.1989	14:28:45	36.98	28.19	93⁰/32⁰/-85⁰	267⁰/58⁰/-93⁰	5.4	15	GCMT
4	27.04.1989	23:06:52	37.03	28.16	92⁰/36⁰/-94⁰	276⁰/54⁰/-87⁰	5.1	14	GCMT
5	28.04.1989	13:30:19	37.02	28.1	90⁰/41⁰/-101⁰	285⁰/50⁰/-80⁰	5.4	8	GCMT
6	03.08.2004	13:11:30	36.85	27.77	74⁰/38⁰/-97⁰	263⁰/52⁰/-84⁰	5.1	11	GCMT
7	04.08.2004	03:01:05	36.83	27.76	75⁰/40⁰/-95⁰	262⁰/50⁰/-85⁰	5.4	9	GCMT
8	04.08.2004	04:19:46	36.83	27.81	71⁰/42⁰/-111⁰	278⁰/52⁰/-73⁰	5.3	13	GCMT
9	04.08.2004	14:18:48	36.84	27.78	75⁰/41⁰/-94⁰	260⁰/49⁰/-87⁰	5.2	8	GCMT
10	20.12.2004	23:02:14	36.93	28.36	105⁰/45⁰/-69⁰	257⁰/48⁰/-109⁰	5.3	8	GCMT
11	10.01.2005	23:48:49	36.85	27.92	110⁰/45⁰/-63⁰	255⁰/51⁰/-114⁰	5.2	8	GCMT
12	11.01.2005	04:35:56	36.89	27.87	100⁰/33⁰/-69⁰	255⁰/60⁰/-103⁰	5.2	10	GCMT
13	08.05.2011	06:50:24	36.7	27.24	60⁰/30⁰/-97⁰	248⁰/61⁰/-86⁰	5.1	11	GCMT
14	04.06.2012	14:19:53	28.16	36.94	107⁰/43⁰/-49⁰	238⁰/58⁰/-122⁰	4.5	6	NOA
15	24.11.2012	21:04:17	36.65	27.98	249⁰/63⁰/-66⁰	335⁰/35⁰/-128⁰	4.1	6	KOERI
16	24.11.2012	21:31:15	36.64	27.93	67⁰/39⁰/-61⁰	211⁰/56⁰/-111⁰	4.0	7	KOERI
17	26.11.2012	17:35:42	36.58	27.95	35⁰/31⁰/-94⁰	219⁰/59⁰/-88⁰	4.7	22	GCMT
18	13.08.2014	09:42:55	36.94	27.70	134⁰/17⁰/-56⁰	278⁰/75⁰/-99⁰	4.1	4	Pınar (KOERI)
19	26.11.2014	05:05:33	36.76	27.84	112⁰/51⁰/-71⁰	263⁰/42⁰/-111⁰	4.2	10	MED_RCMT
20	29.05.2015	08:02:51	36.92	27.61	277⁰/53⁰/-75⁰	74⁰/40⁰/-109⁰	4.0	7	KOERI
21	15.12.2016	16:43:56	37.09	28.64	63⁰/57⁰/-114⁰	282⁰/40⁰/59⁰	4.0	7	AFAD
22	25.01.2017	01:19:32	36.79	27.66	92⁰/29⁰/-70⁰	248⁰/63⁰/-101⁰	4.0	10	AFAD
23	13.04.2017	16:22:15	37.14	28.66	73⁰/37⁰/-117⁰	286⁰/58⁰/-71⁰	4.9	5	GCMT
24	20.07.2017	22:31:09	36.96	27.40	280⁰/50⁰/-79⁰	83⁰/41⁰/-103⁰	6.6	7	This Study

N-S Extensional Stress Tensor

N-S extension

In this study 58 events, comprising new and published focal mechanisms (Tables 1, 2 and 3), are included in the Carey-Gailhardis and Mercier (1987) inversion method in order to obtain present-day stress tensors and their tectonic implications. These are the focal mechanisms for earthquakes that occurred in Gökova and its environs before July 20, 2017 (references in Table 3), as well as the major shock and its aftershocks (see Tables 2 and 3). Figure 10 illustrates the available focal mechanisms for earthquakes with magnitudes ranging from 4.0 to 6.6 between 1933 and 2017 including the 20th July 2017 main event (Mw: 6.6). All focal mechanisms that give normal to oblique slip faulting are introduced into the inversion in order to determine the stress state acting in an area wider than Gökova Gulf. The inversion of 24 selected nodal plane sets (Table 3) yields a normal faulting stress regime (e.g., σ_1 is vertical) characterized by approximately N-S (N356°E) σ_3 axis, i.e. minimum horizontal stress axis (Fig. 11). The computed R value is 0.571 indicating a triaxial extensional stress state and clearly differs from a radial extension stress state, which requires a high R value (R≥0.85) as defined in Bellier and Zoback (1995).

Figure 8 shows the focal mechanisms of 12 aftershocks with magnitude ranging from 3.6 to 4.5 as well as that of the main shock. The inversion of the 13 nodal plane sets (Table 1) gives a normal faulting stress regime with approximately N-S (N5°E) minimum horizontal stress axis (σ_3) (Fig. 11). The determined R value of 0.367 implies a triaxial stress state rather than a radial extension which needs a low R value (R≤0.15) as described by Bellier and Zoback (1995). The inversion of the moment tensor of the 20th July 2017 earthquake (Mw 6.6) yields fault parameters from both nodal planes (NP1: strike, 280˚, dip. 50˚ and rake, -79˚; NP2: 83˚, 41˚, -103˚; see Table 1 for details). The inversion of the focal mechanism algorithm chose NP1 as the suitable fault plane (i.e. the plane that dips to the north) for calculating the convenient stress tensor. Similar to other inversion methods, the analysis we used in this study is an effective and successful method for determining the stress tensor, or stress field orientations, from a population of nodal planes, but it is not capable of determining stress magnitude. Furthermore, even if the algorithm selects one of the nodal planes as the fault plane based on the computed stress tensor, surface rupture and/or aftershock distribution are required to confirm this. Saltogianni et al. (2017) proposed that the Bodrum-Kos earthquake caused a nearly E-to ESE striking rupture in the upper crust from the surface (sea bed) to a depth of 12 km based on seismological and geodetic data. However, no surface ruptures were observed on land. As a result, it is difficult to tell which of the nodal planes is the true fault (i.e. whether the seismic fault dips north or south) based on the available evidence.

The dip and location of the source fault are also debated; those who argue that the fault dips north indicated that the fault is located in the center of the gulf, such as the North Datça Fault extending to the east of Kos (Karasözen et al., 2018) or a fault with 10 km E-W trend following the Gökova Rift (Ganas et al., 2019). The seismic fault is situated in the northwest of the basin, offshore of Kos and Bodrum according to those who suggested the source fault dips south (Saltogianni et al., 2017; Tiryakioğlu et al. 2018; Ocakoğlu et al., 2018). The fault planes measured near Ören town in the middle part of the Gökova Fault as shown in Figure 12, are E-W striking normal faults with high dip angle (80º). Our MT parameters for the 20 July 2017 earthquake, on the other hand, show E-W nodal planes with relatively low dip (Table 1). The current results indicate that the fault that ruptured during the 20 July 2017 earthquake is not the same as the Gökova Fault or its western continuation in the gulf. The disagreements

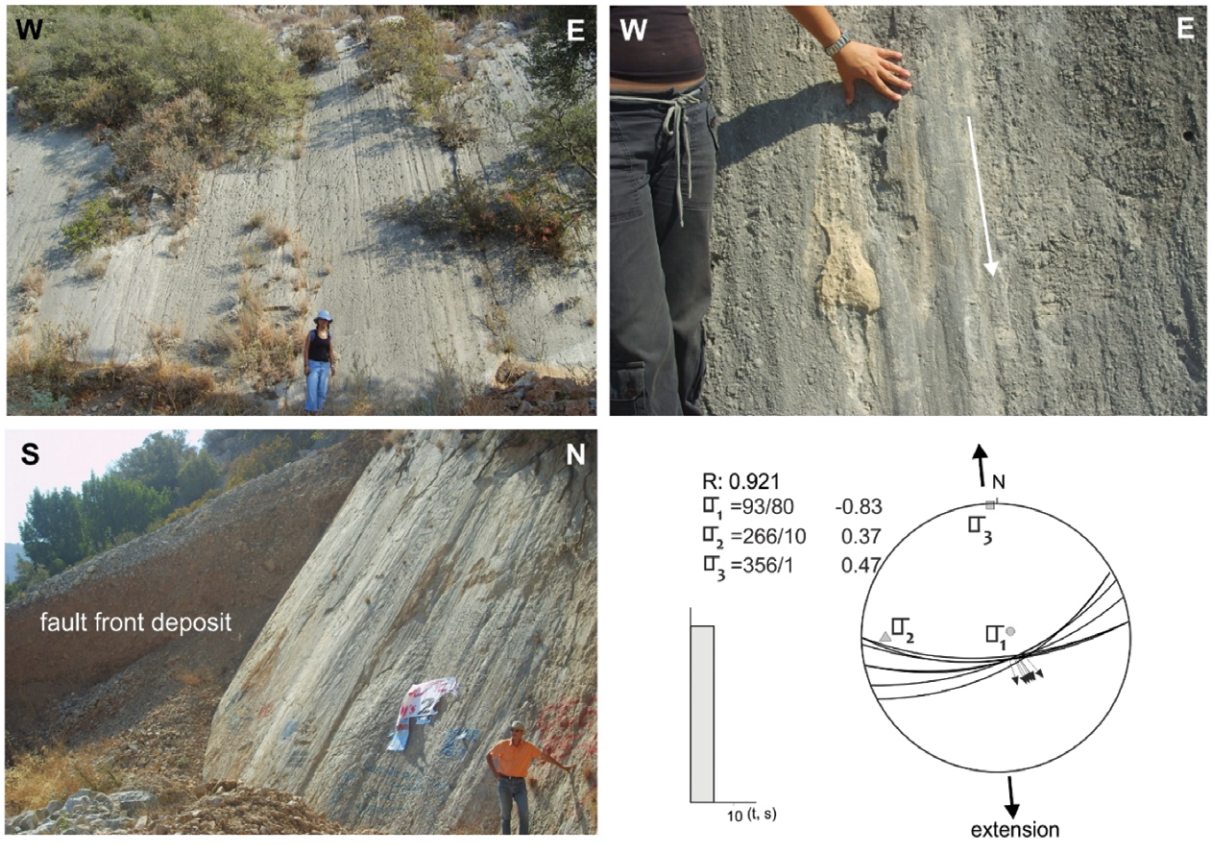

Figure 12. View of metric normal fault planes (Demirtaş, 2008) measured in the central part of the Gökova Fault Zone (UTM: 0582778 E - 4100006 N). Lower hemisphere stereoplots showing inversion results for normal faulting data measured on fault planes. The results were determined by the Carey (1979) method, with azimuth, plunge and relative magnitudes of principal axes ($\sigma1$, $\sigma2$ and $\sigma3$) as well as the stress ratio value [$R = (\sigma2 - \sigma1)/(\sigma3 - \sigma1)$].

about the consequences of the 20 July 2017 earthquake (i.e. the inconsistency of the results and interpretations regarding the fault that ruptured during the earthquake and its dip) show that the basin is quite complex and remains to be further explored.

NW-SE extension

The 21 focal mechanisms of the aftershocks, which range in magnitude from 3.8 to 4.8, are given in Figure 9. The focal mechanisms of the earthquakes show normal to oblique slip faulting (Table 2 and Fig. 9). The inversion of 21 nodal plane sets yields a normal faulting stress regime (σ_1 is vertical) characterized by approximately NW-SE ((N330°E) σ_3 axis, i.e. minimum horizontal stress axis (Table 2 and Fig. 11). The computed R value is 0.45 indicating a triaxial extensional stress state. The approximately NW-SE extension was obtained from the inversion of the aftershock focal mechanisms in the western part of the Gulf of Gökova (Fig. 4). The presence of these normal faults is revealed by seismic-reflection profiles with GPS, land DEM and multibeam bathymetry in the marine area (Tur et al. 2015; Ocakoğlu et al., 2018; Tiryakioğlu et al., 2018). Some of the mapped faults were suggested to have strike-slip character as a result of previous geophysical, multibeam bathymetry, and geodetic studies (Uluğ et al., 2005; İşcan et al., 2013; Ocakoğlu et al., 2018; Tiryakioglu et al., 2018). None of the aftershocks in this analysis are strike-slip faulting; instead, they all are normal faulting to oblique slip (Figs. 8 and 9, and Table 1-2). Based on combined geophysical and geodetic data from land and sea, Tur et al. (2015) demonstrated that the faults mapped as strike-slip faults are normal type faults. They also argued that all faults mapped in the gulf which are associated with the tectonic development of the basin have normal character with distinct directions: 1) NW-SE faults controlling submarine valleys, 2) E-W and 3) approximately NE-SW faults associated with the development of Gökova Basin. A seismic profile taken from the eastern coast of Kos Island in the northwest of Gökova Gulf in the NW-SE direction reveals the presence of listric and synthetic faults (see profile no:3 in Ocakoğlu et al., 2018). These faults are in NE-SW direction, suggesting the existence of NW-SE extension, according to this seismic profile. According to Ocakoğlu et al. (2018), there is decelerated tectonism in this area, and minor extension may be enough to create these structures.

Shah (2015) also found the normal extensional regime in western Anatolia, from N–S to NNE–SSW, suddenly changes direction to NW–SE at the exit of Gökova Gulf, using stress tensor analysis of the earthquakes. Shah (2015) inverted 67 nodal plane sets and found a normal faulting stress regime (σ_1 is vertical) with a NW-SE (N313°E) σ_3 axis, and a R value of 0.39, which supports our findings (Fig. 11). Shah (2015) suggested also that the Gökova area is distinguished by a clockwise rotation of stress directions from N-S to NW-SE. The anticlockwise rotation in the Aegean was also noted in previous geodetic studies (McClusky et al., 2000; Howell et al., 2017). GPS slip vectors (Saltogianni et al., 2017; Tiryakioğlu et al., 2017; Ganas et al., 2019), which show displacements (i.e. horizontal co-seismic displacement) changing direction from N-S to NW-SE, support this faulting process and agree with our findings.

Conclusions

The extensive work of processing the data generated by the main shock and its aftershock activity is presented here to contribute to understanding of the stress regime which is responsible for the deformation in the study area. The results are as follows:

1) The MT solution of the main shock yields approximately E-W striking nodal planes which are compatible with N-S extension. However, the MT solution analysis of aftershock events gives two distinct directions for the nodal planes: approximately E-W and NE-SW to NNE-SSW. The inversion of the focal mechanisms yields N-S extension from E-W nodal planes and NW-SE extension from NE-SW to NNE-SSW nodal planes. The Bodrum-Kos

earthquake (Mw: 6.6) and its aftershocks with E-W focal planes occurred under N-S extension, while the aftershocks related to the approximately NE-SW trending nodal planes were generated under NW-SE extension. The NW-SE extension appears to be local and probably contributes to the growth of the western part of the asymmetric Gökova Basin.

2) The inversion of the focal mechanisms of earthquakes occurring in Gökova Basin and its surrounding areas for the period between 1933 and 2017 yields approximately N-S extension. The N-S extension is also supported by field data. The N-S extension which is responsible for the 20 July 2017 Bodrum-Kos earthquake (6.6 in Mw) seems to be related to African subduction beneath the Aegean.

Acknowledgements

The authors would like to thank Catherine Yiğit for professional editing assistance with English exposition that improved the last version of the text. We also thank the editor and anonymous reviewers for their valuable comments and suggestions, which improved the quality of the manuscript.

References

Akyol, N., Zhu, L., Mitchell, B. J., Sözbilir, H., & Kekovali, K. (2006). Crustal structure and local seismicity in western Anatolia. *Geophysical Journal International,* 166, 1259-1269. https://doi.org/10.1111/j.1365-246X.2006.03053.x

Aktug, B., Nocquet, J. M., Cingöz, A., Parsons, B., Erkan, Y., England, P., … Tekgül, A. (2009). Deformation of western Turkey from a combination of permanent and campaign GPS data: limits to block-like behavior. *Journal of Geophysical Research Atmospheres,* 114(B10), B10404. DOI:10.1029/2008JB006000.

Alçiçek, M. C., Ten Veen, J. H., & Özkul, M. (2006). *Neotectonic development of the Çameli basin, southwestern Anatolia, Turkey.* Geological Society, London, Special Publications, 260(1), 591-611. https://doi.org/10.1144/GSL.SP.2006.260.01.25

Altınok, Y., & Ersoy, Ş. (2000). Tsunamis observed on and near the Turkish coast. *In Natural Hazards*, pp. 185-205. Springer, Dordrecht. DOI:10.1023/A:1008155117243

Ambraseys, N. N. & White, D. (1997). The seismicity of the eastern Mediterranean region 550-1 BC: A re-appraisal. *Journal of Earthquake Engineering*, 1(04), 603-632. https://doi.org/10.1080/13632469708962380

Angelier, J., Dumont, J. F., Karamenderesi, H., Poisson, A., Şimşek, S., & Uysal, S. (1981). Analyses of fault mechanisms and expansion of south-western Anatolia since the Late Miocene. *Tectonophysics,* 75, T1-T9. https://doi.org/10.1016/0040-1951(81)90271-7

Barka, A. (1992). The North Anatolian Fault Zone. *Annales Tectonicae*, 6, 164-195.

Bellier, O. & Zoback, M. (1995). Recent state of stress change in the Walker Lane zone western Basin and Range Province-USA. *Tectonics,* 14, 564-593. https://doi.org/10.1029/94TC00596

Bellier, O., Över, S., Poisson, A., & Andrieux, J. (1997). Recent temporal change in the stress state and modern stress field along North Anatolian Fault Zone (Turkey). *Geophysical Journal International,* 131, 61-86. https://doi.org/10.1111/j.1365-246X.1997.tb00595.x

Biryol, C. B., Beck, S. L., Zandt, G. & Özacar, A. A. (2011). Segmented African lithosphere beneath the Anatolian region inferred from teleseismic P–wave tomography. *Geophysical Journal International,* 184, 1037-1057. https://doi.org/10.1111/j.1365-246X.2010.04910.x

Bott, M. H. P. (1959). The Mechanism of Oblique Slip Faulting. *Geological Magazine,* 96, 109-117. https://doi.org/10.1017/S0016756800059987

Bouchon, M. (1981). A simple method to calculate Green's functions for elastic layered media. *Bulletin of the Seismological Society of America,* 71(4), 959-971. https://doi.org/10.1785/BSSA0710040959

Carey, E. & Brunier, B. (1974). Analyse theorique et numerique d'une modele mechanique elementaire applique a l'etude d'une population de failles. *C.R. Acad. Sci.,* Paris. Ser. D 279, 891-894

Carey, E. (1979). Recherche des directions principales de contraintes associées au jeu d'une population de failles. *Revue Geological Dynamic and Géography Physic,* 21, 57-66.

Carey-Gailhardis, E. & Mercier, J. L. (1987). A numerical method for determining the state of stress using source mechanisms of earthquake populations. *Earth and Planetary Science Letters*, 82, 165-179. https://doi.org/10.1016/0012-821X(87)90117-8

Çevikbilen, S., Taymaz, T., & Helvacı, C. (2014). Earthquake mechanisms in the Gulfs of Gökova, Sığacık, Kuşadası, and the Simav Region (western Turkey): Neotectonics, seismotectonics and geodynamic implications. *Tectonophysics*, 635, 100-124. https://doi.org/10.1016/j.tecto.2014.05.001

Çevikbilen, S. and Taymaz, T. (2012). Earthquake source parameters along the Hellenic subduction zone and numerical simulations of historical tsunamis in the Eastern Mediterranean. *Tectonophysics,* 536, 61-100. https://doi.org/10.1016/j.tecto.2012.02.019

De Boorder, H., Spakman, W., White, S. H. & Wortel, M. J. R. (1998). Late Cenozoic mineralization, orogenic collapse and slab detachment in the European Alpine Belt. *Earth and Planetary Science Letters,* 164, 569-575. https://doi.org/10.1016/S0012-821X(98)00247-7

Demirtaş, Z. (2008). Ören ve civarının genel jeolojik özellikleri. *ÇOMÜ Müh. Fak. Jeoloji. Müh. Bölümü, Bitirme Tezi (Danışman: S. Özden),* 87s., Çanakkale.

Dewey, J. F. & Şengör, A. M. C. (1979). Aegean and surrounding regions: Complex multiplate and continuum tectonics in a convergent zone. *Geological Society of America Bulletin,* 90, 84-92.

Emre, Ö., Duman, T. Y. & Özalp, S. (2013). *1:250.000 Ölçekli Türkiye Diri Fay Haritaları Serisi.* Maden Tetkik ve Arama Genel Müdürlüğü, Ankara Türkiye.

Ergin, K., Güçlü, U. & Uz, Z. (1967). *A Catalog of Earthquakes for Turkey and Surrounding Area (11 A.D. to 1964 A.D.). Technical Report*. İstanbul Technical University, Faculty of Mines, Institute of Physics of the Earth, no. 24.

Eyidoğan, H. & Barka, A. (1996). The 1 October 1995 Dinar earthquake, SW Turkey. *Terra Nova,* 8, 5, 479-485. https://doi.org/10.1111/j.1365-3121.1996.tb00773.x

Ganas, A., Elias, P., Kapetanidis, V., Valkaniotis, S., Briole, P., Kassaras, I., Argyrakis, P., Barberopoulou, A., & Moshou, A. (2019). The July 20, 2017 M6.6 Kos Earthquake: Seismic and Geodetic Evidence for an Active North-Dipping Normal Fault at the Western End of the Gulf of Gökova (SE Aegean Sea). *Pure and Applied Geophysics,* 176, 4177-4211. https://doi.org/10.1007/s00024-019-02154-y

Gephart, J. W. & Forsyth, D. W. (1984). An improved method for determining the regional stress tensor using earthquake focal mechanism data: Application to the San Fernando Earthquake Sequence. *Journal of Geophysical Research*, 89, 9305-9320. https://doi.org/10.1029/JB089iB11p09305

Guidoboni, E., Comastri, A., & Triana, G. (1994). Catalogue of Ancient Earthquakes in the Mediterranean Area up to the10th Century. *Istituto Nazionale di Geofisica,* p. 504. ISBN 88-85213-06-5.

Görür, N., Şengör, A. M. C., Sakınç, M., Akkök, R., Yiğitbaş, E., Oktay, F. Y., … Aykol, A. (1995). Rift formation in the Gökova region, southwest Anatolia: implications for the opening of the Aegean Sea. *Geological Magazine,* 132(6), 637-650. https://doi.org/10.1017/S0016756800018884

Gürer, Ö. F. & Yılmaz, Y. (2002). Geology of the Ören and surrounding regions, SW Turkey. *Turkish Journal of Earth Sciences,* 11, 2-18.

Gürer, Ö. F., Sanğu, E., Özburan, M., Gürbüz, A., & Sarica-Filoreau, N. (2013). Complex basin evolution in the Gökova Gulf region: implications on the Late Cenozoic tectonics of southwest Turkey. *International Journal of Earth Sciences,* 102(8), 2199-2221. https://doi.org/10.1007/s00531-013-0909-1

Heiderzadeh, M., Necmioğlu, O., Ishibe, T., & Yalçıner, A. C. (2017). Bodrum–Kos (Turkey–Greece) Mw 6.6 earthquake and tsunami of 20 July 2017: a test for the Mediterranean tsunami warning system. *Geoscience Letters*, 4, 31. https://doi.org/10.1186/s40562-017-0097-0

Howell, A., Jackson, J., Copley, A., McKenzie, D., & Nissen, E. (2017). Subduction and vertical coastal motions in the eastern Mediterranean. *Geophysical Journal International,* 211, 593-620. https://doi.org/10.1093/gji/ggx307

İşcan, Y., Tur, H., & Gökaşan, E. (2013). Morphologic and seismic features of the Gökova gulf, SW Anatolia: evidence of strike-slip faulting with compression in the Aegean extensional regime. *Geo-Marine Letters,* 33(1), 31-48. https://doi.org/10.1007/s00367-012-0307-x

Jackson, J., & McKenzie, D. P. (1984). Active tectonics of the Alpine-Himalayan belt between western Turkey and Pakistan. *Geophysical Journal Royal Astronomy Society,* 77, 185-264. https://doi.org/10.1111/j.1365-246X.1984.tb01931.x

Jackson, J., & McKenzie, D. P. (1988). The relationship between plate motion and seismic moment tensors, and the rates of active deformation in the Mediterranean and Middle-East. *Geophysical Journal, 93,* 45-73.

Jolivet, L. & Brun, J. P. (2010). Cenozoic geodynamic evolution of the Aegean. *International Journal of Earth Sciences*, 99, 109-138. https://doi.org/10.1007/s00531-008-0366-4

Kalafat, D. & Horasan, G. (2012). A seismological view to Gökova region at southwestern Turkey. *International Journal of Physical Sciences,* 7(30), 5143-5153. https://link.springer.com/article/10.1007/s00531-008-0366-4

Karasözen, E., Nissen, E., Büyükakpınar, P., Cambaz, M. D., Kahraman, M., Ertan, E. S., … Ozacar, A. A. (2018). The 2017 July 20Mw 6.6 Bodrum-Kos earthquake illuminates active faulting in the Gulf of Gökova, SW Turkey. *Geophysical Journal International,* 214, 185-199. https://doi.org/10.1093/gji/ggy114

Kikuchi, M., & Kanamori, H. (1991). Inversion of complex body waves. *Bulletin of the Seismological Society of America,* 81, 2335-2350.

Konca, A. O., Güvercin, S. E., Özarpacı, S., Özdemir, A., Funning, G. J., Doğan, U., … Reilinger, R. (2019). Slip distribution of the 2017 Mw6.6 Bodrum-Kos earthquake: resolving the ambiguity of fault geometry. *Geophysical Journal International,* 219(2), 911-923. https://doi.org/10.1093/gji/ggz332

Kuge, K. (2003). Source modeling using strong-motion waveforms: toward automated determination of earthquake fault planes and moment-release distributions. *Bulletin of the Seismological Society of America,* 93, 639-654. DOI:10.1785/0120020076

Kurt, H., Demirbağ, E., & Kuşçu, İ. (1999). Investigation of the submarine active tectonism in the Gulf of Gökova, southwest Anatolia–southeast Aegean Sea, by multi-channel seismic reflection data. *Tectonophysics,* 305, 477-496. https://doi.org/10.1016/S0040-1951(99)00037-2

Le Pichon, X., & Angelier, J. (1979). The Hellenic arc and trench system: a key to the evolution of eastern Mediterranean area. *Tectonophysics,* 60, 1-42. https://doi.org/10.1016/0040-1951(79)90131-8

Le Pichon, X., Chamot-Rooke, N., Lallemant, S., Noomen, R., & Veis, G. (1995). Geodetic determination of kinematics of central Greecewith respect to Europe: implication for eastern Mediterranean tectonics. *Journal of Geophysical Research Atmospheres,* 100, 12675-12690.

Luttrell, A. (1999). *Earthquakes in the Dodecanese: 1303–1512*. In: E. Zachariadon (Ed.). *Natural Disasters in the Ottoman Empire (Rethymnon, 1999)*, repr. in Luttrell, Studies, no. X, 145-51.

McClusky, S., Balassanian, S., Barka, A., and et al. (2000). Global Positioning System constraints on plate kinematics and dynamics in the eastern Mediterranean and Caucasus. *Journal of Geophysical Research,* 105(B3), 5695-5719. https://doi.org/10.1029/1999JB900351

McKenzie, D. P. (1972). Active tectonics of the Mediterranean region. *Geophysical Journal of the Astronomical Society,* 55, 217-254. https://doi.org/10.1111/j.1365-246X.1972.tb02351.x

Mercier, J. L., Sorel, D., & Vergely, P. (1989). Extensional tectonic regimes in the Aegean basins during the Cenozoic. *Basin Research,* 2, 49-71. https://doi.org/10.1111/j.1365-2117.1989.tb00026.x

Mercier, J. L., Carey-Gailhardis, E., & Sebrier, M. (1991). Paleostress determinations from fault kinematics: application to the Neotectonics of the Himalayas-Tibet and the Central Andes. *Philosophical Transactions of the Royal Society*, 337, 41-52. https://doi.org/10.1098/rsta.1991.0105

Oral, M. B., Robert, E. R., Toksöz, N. M., King, R. W., Barka, A. A., Kınık, I., & Lenk, O. (1995). Global Positioning System offers evidence of plate motions in Eastern Mediterranean. *Eos, Transactions American Geophysical Union 76*, (2), 9-11. DOI: 10.1029/EO076i002p00009-01

Ocakoğlu, N., Nomikou, P., İşcan, Y., Loreto, M. F. & Lampridou, D. (2018). Evidence of extensional and strike-slip deformation in the offshore Gökova-Kos area affected by the July 2017 Mw6. 6 Bodrum-Kos earthquake, eastern Aegean Sea. *Geo-Marine Letters,* 38(3), 211-225. https://doi.org/10.1007/s00367-017-0532-4

Över, S., Özden, S., Pınar, A., Yılmaz, H., Ünlügenç, U. C. & Kamacı, Z. (2010). Late Cenozoic Stress Field in the Çameli Basin, SW Turkey. *Tectonophysics,* 492, 1-4, 60-72. DOI:10.1016/j.tecto.2010.04.037

Över, S., Özden, S., Pınar, A., Yılmaz, H., Kamaci, Z. & Ünlügenç, U. C. (2016). Late Cenozoic Stress State distributions at the intersection of the Hellenic and Cyprus Arcs, SW Turkey. *Journal of Asian Earth Sciences, 132,* 94-102. DOI:10.1016/j.jseaes.2016.10.003

Özden, S., Över, S., Poyraz, S. A., Güneş, Y., & Pınar, A. (2018). Tectonic implications of the 2017 Ayvacık (Çanakkale) earthquakes, Biga Peninsula, NW Turkey. *Journal of Asian Earth Sciences,* 154, 125-141. https://doi.org/10.1016/j.jseaes.2017.12.021

Reilinger, R., McClusky, S., Vernant, P., Lawrence, S., Ergintav, S., Cakmak, R., … Karam, G. (2006). GPS constraints on continental deformation in the Africa–Arabia–Eurasia continental collision zone and implications for the dynamics of plate interactions. *Journal of Geophysical Research*, 111(B5). https://doi.org/10.1029/2005JB004051

Reilinger, R., McClusky, S., Paradissis, D., Ergintav, S., & Vernant, P. (2010). Geodetic constraints on the tectonic evolution of the Aegean region and strain accumulation along the Hellenic subduction zone. *Tectonophysics,* 488, 22-30. https://doi.org/10.1016/j.tecto.2009.05.027

Saltogianni, V., Taymaz, T., Yolsal-Çevikbilen, S., Eken, T., Moschas, F., & Stiros, S. (2017). Fault model fort the 205 Leucas (Aegean Arc) Earthquake: Analysis based on seismological and geodetic observations. *Bulletin of the Seismological Society of America,* 107(1), 433-444. DOI: 10.1785/0120160080

Sebrier, M., Mercier, J. L., Machare, J., Bonnot, D., Cabrera, J., & Blanc, J. L. (1988). The state of stress in an overridding plate situated above a flat slab: The Andes of central Peru. *Tectonics*, 7, 895-928.

Shah, S. T. (2015). *Stress tensor inversion from focal mechanism solutions and earthquake probability analysis of western Anatolia*. MSc Thesis, School of Natural and Applied Sciences, Middle East Technical University, Ankara, Turkey.

Sokos, E., & Zahradnik, J. (2008). ISOLA a FORTRAN code and MATLAB GUI to perform multiple point source inversion of seismic data. *Computers and Geosciences,* 34, 976-977. https://doi.org/10.1016/j.cageo.2007.07.005

Şaroğlu, F., Emre, Ö., & Kuşçu, İ. (1992). *Türkiye diri fay haritası: Active fault map of Turkey*. Maden Tetkik ve Arama Genel Müdürlüğü, Ankara.

Taymaz, T., Jackson, J., & Westaway, R. (1990). Earthquake Mechanisms in the Hellenic Trench near Crete. *Geophysical Journal International,* 102(3), 695-731. https://doi.org/10.1111/j.1365-246X.1990.tb04590.x

Taymaz, T., Jackson, J., & Mc Kenzie, D. (1991). Active tectonics of the north and central Aegean Sea. *Geophysical Journal International,* 106, 2, 433-490.

Tiryakioğlu, İ, Aktuğ, B., Yiğit, C. Ö., Yavaşoğlu, H., Sözbilir, H., Özkaymak, Ç., … Özener, H. (2018). Slip distribution and source parameters

of the 20 July 2017 Bodrum-Kos earthquake (Mw 6.6) from GPS observations. *Geodinamica Acta,* 30 (1), 1-14. https://doi.org/10.1080/09853111.2017.1408264

Tur, H., Yaltırak, C., Elitez, İ., & Sarkavak Tuncer, K. (2015). Pliocene–Quaternary tectonic evolution of the Gulf of Gökova, southwest Turkey. *Tectonophysics,* 638, 158-176. DOI:10.1016/j.tecto.2014.11.008

Uluğ, A., Duman, M., Ersoy, Ş., Özel, E., & Avcı, M. (2005). Late Quaternary sea-level change, sedimentation and neotectonics of the Gulf of Gökova: Southeastern Aegean Sea. *Marine Geology,* 221(1-4), 381-395. DOI:10.1016/j.margeo.2005.03.002

Vasseur, G., Bernard, P., Van de Meulebrouck, J., Kast, Y., & Jolivet, J. (1983). Component parts of the World Heat Flow Data Collection. *Pangaea*. https://doi.org/10.1594/PANGAEA.806246.

Yalçıner, A. C., Annunziato, A., Papadopoulos, G., Dogan, G. G., Guler, H. G., Cakır, T. E., … Synolakis, C. (2017). The 20th July 2017(22:31 UTC) Bodrum/Kos earthquake and tsunami; post tsunami field survey report, July 27 2017, Istanbul, Turkey. *Pure and Applied Geophysics, 176(1).* DOI:10.1007/s00024-019-02151-1

Yolsal, S., Taymaz, T., & Yalçıner, A. C. (2007). Understanding tsunamis, potential source regions and tsunami prone mechanisms in the Eastern Mediterranean. *Geological Society London Special Publications,* 291, 201–230, DOI:10.1144/SP291.10.

Yolsal, S., & Taymaz, T. (2010). Source Mechanism Parameters of Gulf Of Gökova Earthquakes and Tsunami Risk in the Rodos-Dalaman Region. *İTÜ Dergisi* /d 9 (3), İstanbul Technical University, İstanbul pp. 53-65.